

SUPPLEMENTARY INFORMATION

Fluorescence Interference Contrast-enabled micro/nano-structured microarrays

S. Dobroiu, F. van Delft, J. Aveyard-Hanson, P. Shetty, D.V. Nicolau*

1. Fluorescence Interference Contrast (FLIC) theory

Standing wave effect

The central phenomenon leading to the modulation of fluorescence by calibrated layers on a substrate is the standing wave effect, classically observed and used in optical lithography (Levinson 2005). When a punctual source of light, e.g., an emitting fluorophore molecule, is placed at a distance from a reflecting layer, that distance modulates the overall intensity of light reflected by the bottom layer.

The relative phase difference between two or more waves is given by the relative optical path length difference, where the optical path length is given by the product between geometrical path length and the refraction index of the medium that the light traverses. For a beam of light A

$$A = A_0 \sin(kx - \omega t)$$

the phase is given by the term between brackets

$$\phi_A = kz - \omega t$$

where z gives the spatial coordinate.

For a second beam B with the source displayed by a quantity h and passing through a medium with a refractive index n

$$B = B_0 \sin[k(z - nh) - \omega t]$$

the phase being

$$\phi_B = k(z - nh) - \omega t$$

the relative phase difference between beams A and B will be

$$\phi_A - \phi_B = knh$$

Because the wavenumber k is given by

$$k = \frac{2\pi}{\lambda}$$

where λ is the wavelength, then the relative phase difference becomes

$$\phi_A - \phi_B = \frac{2\pi}{\lambda} nh$$

and the condition for maximum constructive interference is achieved when the phase difference is a multiple integer of 2π (or one wavelength) while maximum destructive interference is achieved at a phase difference multiple of π (or half a wavelength).

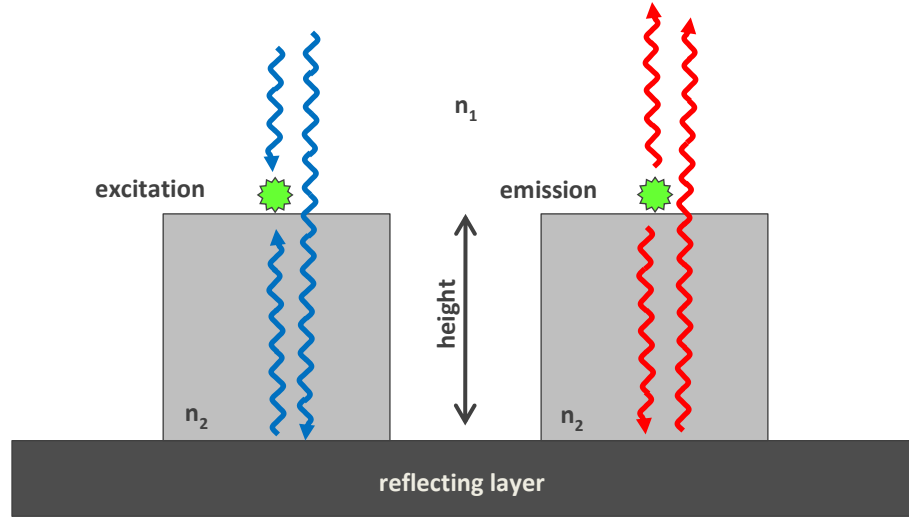


Figure SI 1. Geometrical and optical environment in which FLIC phenomenon occurs.

In the setup above, the direct excitation light will interfere with its reflection giving rise to a standing wave, and the same is valid for the emitted light. The phase difference between the direct and the reflected beams will be given, in this case, by

$$\phi_{ex} = \frac{2\pi}{\lambda} 2(n_1 h + n_2 h_2)$$

Because the medium characterized by a refractive index n_1 is air and the medium characterized by the refractive index n_2 is SiO_2 with the thickness h_{SiO_2} , the relative phase difference becomes

$$\phi_{ex} = \frac{4\pi}{\lambda} n_{\text{SiO}_2} h_{\text{SiO}_2}$$

Or, in the case of emitted light, such as from a fluorophore (Figure SI 1, right)

$$\phi_{em} = \frac{4\pi}{\lambda} n_{\text{SiO}_2} h_{\text{SiO}_2}$$

Fluorescence Interference Contrast

As it can be inferred from the explanations above, when a fluorophore is placed in the vicinity, e.g., tens to hundreds of nanometres away, of a reflecting surface part of the excitation light is reflected and interferes with the incoming wave. By varying the distance between the emitter, i.e., the fluorophore, and the reflector, i.e., the reflecting surface, an amplification, or suppression, of the intensity of fluorescence can be achieved. The physical and mathematical framework of the process has been classically reported before (Brandstatter et al. 1988; Nakache et al. 1985). Using a monolayer of fluorescent molecules on SiO_2 terraces, it was demonstrated (Lambacher and Fromherz 1996) that the principles of classical optics sufficiently explain the modulation of the intensity of fluorescence signals. Based on this observation, the FLIC technique was proposed (Lambacher and Fromherz 1996), which is capable of accurately measuring nanometre-scale distances on the z-axis (Lambacher and Fromherz 2002). In the original FLIC experiment, the intensity values of the fluorescence emission obtained using a substrate inducing interference effects, i.e. formation of standing waves, are fitted on a curve

describing the relationship between the unknown effective optical paths, i.e., thickness of the substrate layer, and the excitation and emission wavelengths (Brandstatter et al. 1988). Provided that the refraction indices corresponding to the effective optical path segments are known, the distances can be accurately measured.

The mathematical treatment of the optical model of FLIC has been extensively described (Parthasarathy and Groves 2004). A model, which accounts for the formation of standing waves as direct and reflected excitation and emission light, respectively, interfere, is developed towards a more realistic albeit more complex model, which considers the impact of (i) imperfect reflection, (ii) non-normal light incidence, (iii) fluorophore orientation and (iv) light polarization. This model relates the observed fluorescence to the fluorophore – reflector separation distance and the parameters of the function are the refractive indices of the media traversed by light, the reflectivity coefficient of the reflector and the excitation and emission light wavelengths respectively:

$$F_{exp} \propto \sin^2\left(\frac{2\pi nh}{\lambda_{ex}}\right) \sin^2\left(\frac{2\pi nh}{\lambda_{em}}\right)$$

or, taking into account the reflectivity coefficient, r :

$$F_{exp} \propto [(1 - r_{ex})^2 + 4r_{ex}\sin^2\left(\frac{2\pi nh}{\lambda_{ex}}\right)][(1 - r_{em})^2 + 4r_{em}\sin^2\left(\frac{2\pi nh}{\lambda_{em}}\right)]$$

while for a stack comprised of silicon oxide and titanium oxide, the equation simply becomes:

$$F_{exp} \propto [(1 - r_{ex})^2 + 4r_{ex}\sin^2\left(\frac{2\pi(n_{SiO_2}h_{SiO_2} + n_{TiO_2}h_{TiO_2})}{\lambda_{ex}}\right)][(1 - r_{em})^2 + 4r_{em}\sin^2\left(\frac{2\pi(n_{SiO_2}h_{SiO_2} + n_{TiO_2}h_{TiO_2})}{\lambda_{em}}\right)]$$

Experimental fluorescence intensity data can be fitted with a function accounting for the fluorescence level measured at the reflectors surface, F_0 and a proportionality factor F :

$$F_{exp} = F_0 + F[(1 - r_{ex})^2 + 4r_{ex}\sin^2\left(\frac{2\pi nh}{\lambda_{ex}}\right)][(1 - r_{em})^2 + 4r_{em}\sin^2\left(\frac{2\pi nh}{\lambda_{em}}\right)]$$

It follows that, for a set of (i) transparent material (e.g., SiO_2), manifested in the refractive index, n , for both the emission and excitation light (assuming that n is the same for both wavelengths); (ii) reflecting material (e.g., Si), manifested by the reflectivity for both the emission and excitation light; and (iii) the medium (most of the time, air); as well as a pair of wavelengths for the emission and excitation, the overall intensity of the fluorescence signal will vary as an attenuated sinusoid with the thickness of the transparent layer as a variable.

With this mathematical model framework, different wavelengths of the light emitted by the fluorophore on the top of the spacer will result in various shifted sinusoids, as presented in Figure SI 2

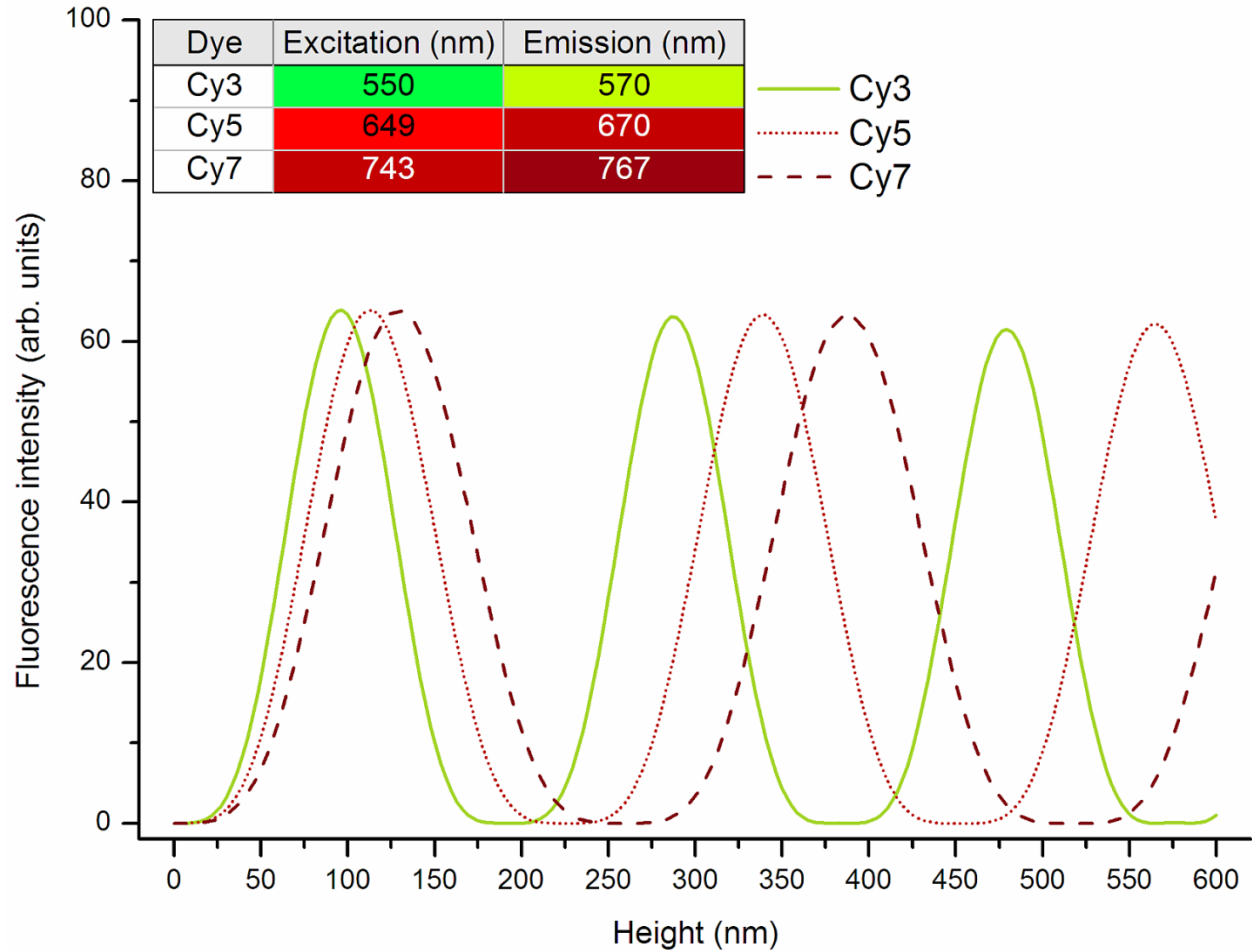


Figure SI 2. Modulation of the emission fluorescence by FLIC for various fluorophores and for various heights (thickness) of the spacer (SiO_2) keeping the fluorophore away from the reflecting layer (Si).

2. Fabrication and analysis of the micro/nano-structured microarray surfaces

The detailed fabrication process for micro/nanostructured surfaces is as follows:

- 25x 4 in. Si wafers
- short sputter etch with Ar^+ shortly before deposition, Veeco Nexus800 Ar 50sccm 6mTorr 500W 45s
- sputter deposition Ti 10 nm (optional adhesion layer, as interface between Pt and SiO_2), Veeco Nexus800 Ar 50sccm 1.67mTorr 250W 40s
- sputter deposition Pt 100 nm, Veeco Nexus800 Ar 140sccm 20mTorr 500W 80s
- sputter deposition TiO_2 100 – 20 nm, Veeco Nexus800 Ar 50+ O_2 35 sccm 4mTorr 2000W 664-133s
- sputter deposition SiO_2 100 – 20 nm, Veeco Nexus800 Ar 50+ O_2 35 sccm 4mTorr 2000W 664-133s
- spin coat 1.5 μm HPR504 resist
- soft bake 2min at 90°C
- exposure stepper $\lambda = 365\text{nm}$, D 100 mJ/cm^2 test reticule mask

- j) develop TMAOH 2min at 21°C
- k) rinse H₂O
- l) spin dry
- m) Optical inspection
- n) RIE in .CHF₃ plasma until interferometer endpoint; + 10% over-etch; wafer-by-wafer; + 30s preliminary resist strip in O₂/N₂ plasma all (to remove “Teflon”)
- o) Optical inspection
- p) Resist strip in Microstrip5010 (N-methyl-2-pyrrolidone, ethanolamine, lactic acid), 10min+5min; + rinse IPA 5min, water 5 min, + spin dry
- q) Optical inspection + α -step profile depth measurement

3. Functionalization of the FLIC-enabled micro/nano-structures

Reagents

The reagents used were as follows. Bovine serum albumin (BSA) and (3-aminopropyl)triethoxysilane, APTES, and (3-Glycidyloxypropyl)trimethoxysilane, GPTES, were purchased from Sigma Aldrich. DyLight 649 (N-hydroxysuccinimidyl functionalized dye) was purchased from Thermo Scientific. Solutions: PBS: 15 mM sodium phosphate, 0.15 M NaCl, pH 7.4. Bicarbonate buffer: 0.1 M sodium bicarbonate, pH 8.2. Wash buffer 1: bicarbonate buffer containing 10% ethanol; Wash buffer 2: PBS containing 0.05 % tween20. De-ionized water used throughout the experiments was obtained via a Millipore water purification system. The following reagents, analytical grade purity, were purchased from Sigma Aldrich: acetone, 2-propanol, ethanol amine, bovine serum albumin (BSA), betaine, di-sodium phosphate, sodium chloride, Tris base, Triton X-100, sodium dodecyl sulfate (SDS), sodium citrate saline (SSC) powder, hydrochloric acid, potassium chloride. 64-well silicone dividers (Grace Biolabs, USA) were also purchased from Sigma Aldrich (UK). The epoxy-silane 3-glycidyloxypropyl triethoxysilane (GPTES) was purchased from Fluorochem (Hadfield, UK). DyLight649-BSA was a gift from Dr. Robert Wilson. Synthetic oligonucleotides with the probe and target sequence 5' CCTCAAAGAGAGAGAAGAAGAAA 3', with a C6 amine modifier at the 5' end, and 5' TTTCTTCTTCTCTCTTTGAGG 3', with a Cy5 modification at the 5' end, respectively, were purchased from Eurogentec (Liège, Belgium).

Aminosilanisation and fluorescent dye functionalisation

The microarray surfaces were incubated on a rocker plate with ethanol/4.25 M acetic acid/APTES (95:3:2) at room temperature for 2 hours. At the end of this period, the surfaces were washed 4 times with ethanol and cured by placing them in an oven at 110°C for 40 minutes. To attach the fluorescent dye, aminosilanised wafers were slow-tilt rotated at room temperature for 4 hours with 10 μ M solution of NHS ester derivatised fluorescent dye (Figure 1C). At the end of this time the wafers were washed once for 5 min in wash buffer 1 and 3 times for 5 min in wash buffer 2 before air drying. Images were obtained using a Zeiss Observer microscope equipped with a LSM 510 laser scanning confocal module.

GPTES-based protocol

The optimization of the coating conditions relied on three methodologies: measurement of contact angles, fluorescence-inferred binding capacity, and surface physical properties. The change in surface hydrophobicity was monitored through contact angle measurements (Figure SI 3) to determine the silane concentration yielding maximum hydrophobicity.

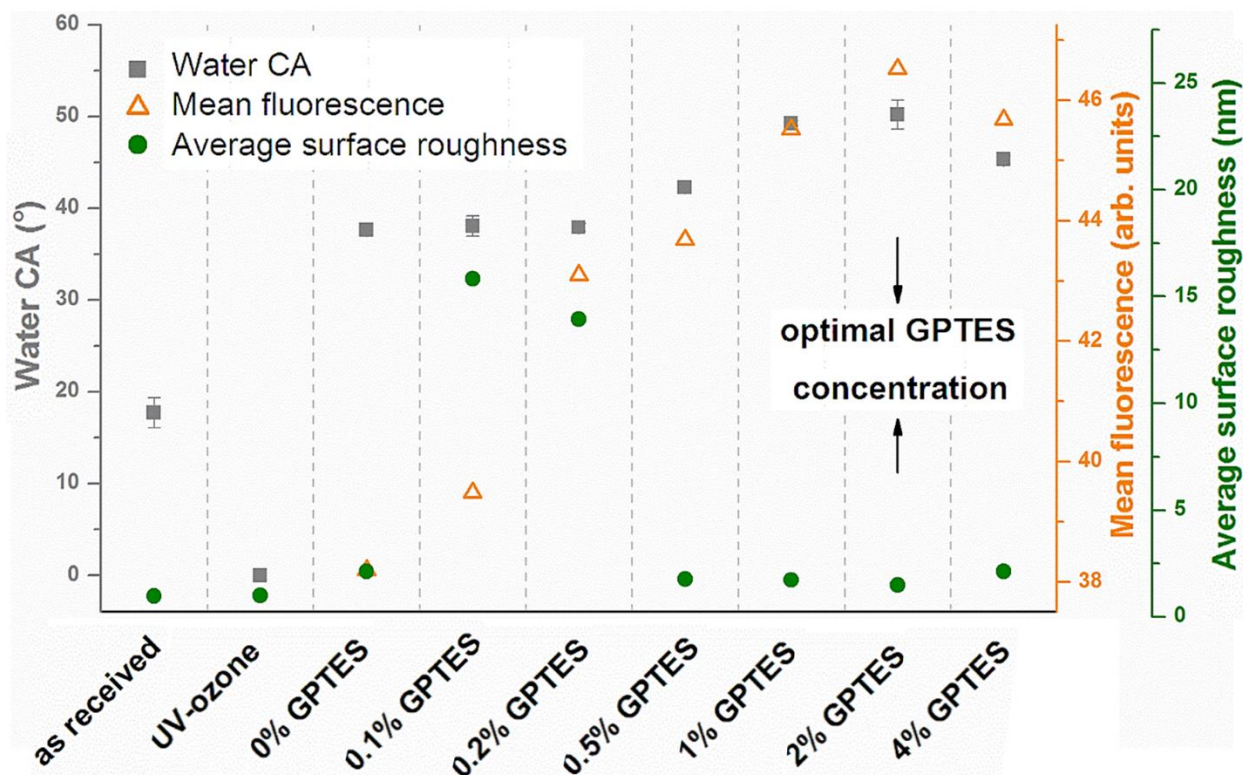


Figure SI 3. Optimal surface chemistry modification procedure as determined via water contact angle, surface roughness and binding capacity measurements.

The surfaces that were treated with GPTES in toluene initially appeared to be ‘immune’ to the low GPTES concentrations, i.e. no significant change in surface hydrophobicity, then a steep increase in the contact angle was observed, from 42° to 50°, respectively, for GPTES concentrations between 0.5 and 2.0%, respectively. These findings are in agreement with available data (Luzinov et al. 2000), albeit for the methoxy homologue of GPTES. For a 4% GPTES concentration, the contact angle drops down to 45° probably due to the formation of polymerized silane aggregates which contribute to the increase of the surface roughness which, in turn, leads to an increase in the wettability of the glass surface.

By using a DyLight649-BSA as a fluorescent probe one can monitor the change in binding capacity of the surface, and by extension the availability of surface epoxy groups, since the BSA molecule has both free amine (Habeeb 1966) and thiol (Oblak et al. 2004) groups that can react with surface epoxide groups. It was found that the average fluorescence intensity from spots printed with DyLight649-BSA follows the same trend as the change in surface hydrophobicity

with the increase in GPTES concentration (Figure SI 3). The maximum fluorescence intensity was obtained for substrates treated with 2% GPTES.

Finally, the average surface roughness measured by tapping mode AFM was used as a surface quality metric. The roughness parameters increase sharply when the GPTES concentration is low, but then start to decrease as the concentration of the silane increases (Figure SI 3). Low values of the surface roughness parameters are measured for an initial silane concentration of 1 and 2% respectively, followed by a slight increase. This can be explained as follows. At the beginning, the surface is topographically homogeneous, with low roughness parameters, but the addition of the silane slowly promotes the formation of islands of silane, thus increasing the surface nano-roughness. In the first stages of this process, the apparent surface hydrophobicity, as measured by contact angles, does not increase substantially because the surface roughness remains in the low nm and islands-like regime. As the silane film starts to cover more of the surface, the roughness decreases to a level that is comparable to that measured before chemical treatment, when the surface topography was homogeneous, as characterized by the local minimum in surface roughness. A further increase in surface roughness could be the result of additional layer formation, probably less ordered since the surface silanol groups are now shielded from the adsorbing molecules. Further, the surface roughness drops and then stabilizes, suggesting that surface topographical homogeneity was reached at a 2% silane concentration.

The sequence of analysis techniques used thus far, i.e., water contact angle measurements, topography and phase contrast imaging and fluorescence imaging, indicates that the optimum deposition process for the epoxy-silane film, based on a deposition time of two hours and a one hour annealing time at 120°C, is achieved using a 2% GPTES concentration.

Chemical analysis of the various surfaces

The noise of the fluorescence signal has its sources, in part, in the heterogeneous wetting and quenching effects at high local concentrations of fluorophores, but an important source of the fluorescence noise lies in the uneven distribution of fluorophore on the surface of the substrates, specifically on the exposed reflectors (for both types of substrates, FLIC structures are made of SiO₂, so any inhomogeneity in surface chemistry is highly unlikely). After the pattern transfer stage of the semiconductor fabrication, i.e., the etch step, fluorocarbon residues are expected to be found on the exposed areas, and they could be the first source of chemical contrast between the top of the FLIC structures and the surrounding background. These contaminants are however removed in the latter low oxygen pressure plasma ashing step, leaving behind a bare silicon surface (which rapidly grows a layer of oxide).

A static-SIMS analysis reveals the presence of mass signals associated to platinum oxide on the surface of the platinum reflector. Also, the standard deviation of the fluorescence intensity measured on the reflectors is smaller for the silicon than for the platinum surfaces. This could be considered a side-effect of the better reflectivity of platinum, but the standard deviation of the signal should scale up with the mean intensity. Another plausible explanation is that, despite the presence of platinum oxide, a “patchy” rather than continuous film is formed on the metal surface which leads to slightly decreased uniformity.

The relative ion abundance table from TOF-SSIMS measurement is presented in Table SI 1.

Table SI 1. TOF-SSIMS measurements of the SLIC enabled structures

Polarity :P		CtMass	Pt	+APTES	+dye	SiO2	+APTES
No.	Ion		#375	#379	#383	#378	#382
1	H	1.0083	74691	56037	72509	152075	64718
2	Li	7.0158	384	5	239	492	4
3	B	11.0089	133	16	126	1075	77
4	C	11.9992	7879	1985	9324	11475	2614
5	CH	13.0066	13730	5016	12501	16616	6399
6	CH ₂	14.0145	27432	21236	20402	37032	24322
7	CH ₃	15.0233	82294	53033	26846	79617	46995
8	O	15.9929	743	134	663	4149	118
9	OH	17.0009	570	121	458	6678	95
10	NH ₄	18.0354	36668	25	958	3898	54
11	F	18.9972	85	4	277	113	5
12	Na	22.9873	495049	7750	786803	601149	3846
13	Mg	23.981	6245	85	1346	1389	122
14	Al	26.9787	8335	1180	38132	67600	9415
15	C ₂ H ₃	27.0233	488846	24058	89154	272493	21663
16	Si	27.973	3481	643753	306713	2894126	605531
17	CHO	29.0005	72269	3794	8736	30433	4578
18	C ₂ H ₅	29.04	357881	4822	19940	112022	4578
19	CH ₃ O	31.0179	96832	2800	1447	18947	3531
20	K	38.9592	209492	785	12095	174804	1746
21	Ca	39.9537	121936	1442	30900	31470	354
22	C ₃ H ₅	41.0388	874557	5281	42966	337291	5366
23	SiCH ₃	42.9964	5246	549816	33036	119272	443529
24	C ₃ H ₇	43.0556	471059	1420	6266	100605	1863
25	SiO	43.9649	1868	3670	7350	65780	2445
26	SiHO	44.9744	3239	36860	90673	921152	29539
27	C ₂ H ₅ O	45.0323	69029	4629	635	4709	14161
28	C ₂ H ₈ N	46.0641	3725	38	25	723	78
29	Cr	51.9277	4358	283	748	597	23
30	C ₄ H ₄	52.0271	55855	300	11210	27862	229
31	Fe	55.9232	153477	8174	9874	28747	2206
32	⁵⁸ Ni	57.9218	65696	1482	1847	6085	300
33	SiC ₂ H ₆	58.0186	3159	40637	564	8061	34563
34	SiC ₂ H ₇	59.031	11343	46765	472	8105	41488
35	SiHO ₂	60.9676	1344	89	470	6723	65
36	C ₅ H ₅	65.0347	129332	476	11698	45774	418
37	C ₄ H ₇ O	71.0468	151365	358	113	2598	941
38	SiC ₃ H ₉	73.0427	37908	125411	418	24961	217250
39	Si ₂ CH ₃ O	86.9631	2606	13747	447	2055	12783
40	C ₇ H ₅	89.0278	49789	931	4430	9383	1871
41	C ₇ H ₇	91.0485	705446	684	12325	62110	611
42	C ₇ H ₁₁	95.0854	62510	67	530	7611	145
43	¹⁹⁵ Pt	194.9183	5591	966	2901	648	348
44	PtC	206.9485	39392	4033	4093	3387	441
45	¹⁹⁵ PtO	210.9583	8865	412	540	577	58

Capture probe printing, surface blocking, and hybridization

Printing of the capture probes was carried out generally following the protocol recommended by Schott for their epoxy slides. The lyophilized oligonucleotide was reconstituted in Millipore deionized water to reach a final concentration of 333.3 μM . This stock solution was used to prepare a 10 μM probe concentration in PBS buffer 0.1M, pH = 9.0, containing 0.15 M NaCl and 1.5 M betaine. Printing was carried out using 0.5 μL capacity split head printing pins. The printed substrates were then incubated for two hours in a humidity chamber and then one hour at 60°C in Pyrex Petri dishes whose bottom was previously lined with filter paper and wetted with a saturated NaCl solution. Removal of the unbound probes was carried out in 4 rinsing steps: 5 minutes in a 0.1% Triton X-100 aqueous solution, two 2 minutes washes in 1 mM HCl solution, a 10 minutes wash in 10 mM KCl solution and, finally, a 1 minute wash in de-ionized water. All washes were carried out using a sufficiently large volume of liquid, following the protocol guidelines. Surface blocking was carried out using a solution containing 50 mM ethanolamine and 0.01% SDS in 0.1 M Tris buffer, pH = 9.0. The slides were incubated for 15 minutes in the blocking solution (a minimum of 100 mL blocking solution per 5 slides), on a water bath at 50°C. The slides were then rinsed in de-ionized water for 1 minute.

Multiple target concentrations were used in hybridization experiments. Before hybridization experiments, 64-well silicone dividers were affixed to the substrates, where each well had a capacity of 22.05 μL . The lyophilized target sequence powder was reconstituted in 893 μL de-ionized water to yield a 100 μM target stock. The hybridization was carried out using solutions containing different target concentrations obtained through serial 5-fold dilutions, from 1 to 3.2 x 10⁻¹¹ μM . The hybridization solutions were prepared so the hybridization buffer (4 x SSC buffer containing 0.1 % SDS) content in the final solution would exceed 90%. A 10 μL volume of target was delivered to each well and the slides were incubated overnight (16 hours) at room temperature in a humidity chamber. Post hybridization washes were carried out for 10 minutes as per the Schott protocol (2x SSC buffer containing 0.2% SDS, 2x SSC buffer and finally 0.2 x SSC buffer). After washing, the slides were dried in a gentle stream of nitrogen.

4. Optimization of the design of the micro/nano-structured microarray surfaces

4.1. Fitting experimental data to the semi-empirical FLIC model

In our study we used as a framework the model accounting for imperfect reflectivity only, since we found that this model describes well, for the first amplification cycle, the fluorescence intensity profile vs. the fluorophore-reflector distance. Additionally, the differences in the fluorescence intensity observed on the structures with the same height, but with different footprints, are accounted by a shape factor, k :

$$F_{\text{exp}} = F_0 + kF[(1 - r_{\text{ex}})^2 + 4r_{\text{ex}} \sin^2(\frac{2\pi nh}{\lambda_{\text{ex}}})][(1 - r_{\text{em}})^2 + 4r_{\text{em}} \sin^2(\frac{2\pi nh}{\lambda_{\text{em}}})]$$

where F_{exp} is the observed fluorescence intensity; F_0 is the residual fluorescence at the surface (zero height) λ_{ex} and λ_{em} are the excitation and emission wavelengths, respectively; n is the index of refraction of the medium that light passes through; h is the reflector-fluorophore distance and

r_{ex} and r_{em} are reflection coefficients of the reflector material at the excitation and emission wavelengths respectively. Further, terms with unknown magnitudes, e.g., angles of incidence of the excitation and emission light, fluorophore orientation and light polarization were all included in a proportionality factor F . The difficulty of fitting of this equation to the experimental data is drastically reduced by the fact that the sinusoidal nature of the correlation between fluorescence intensity vs. the distance between the fluorophore and the reflecting surface has been comprehensively demonstrated before, including using several fluorophores. This established theoretical framework allows the correlations between the fluorescence signal and the geometrical parameters of the FLIC-enabled structures.

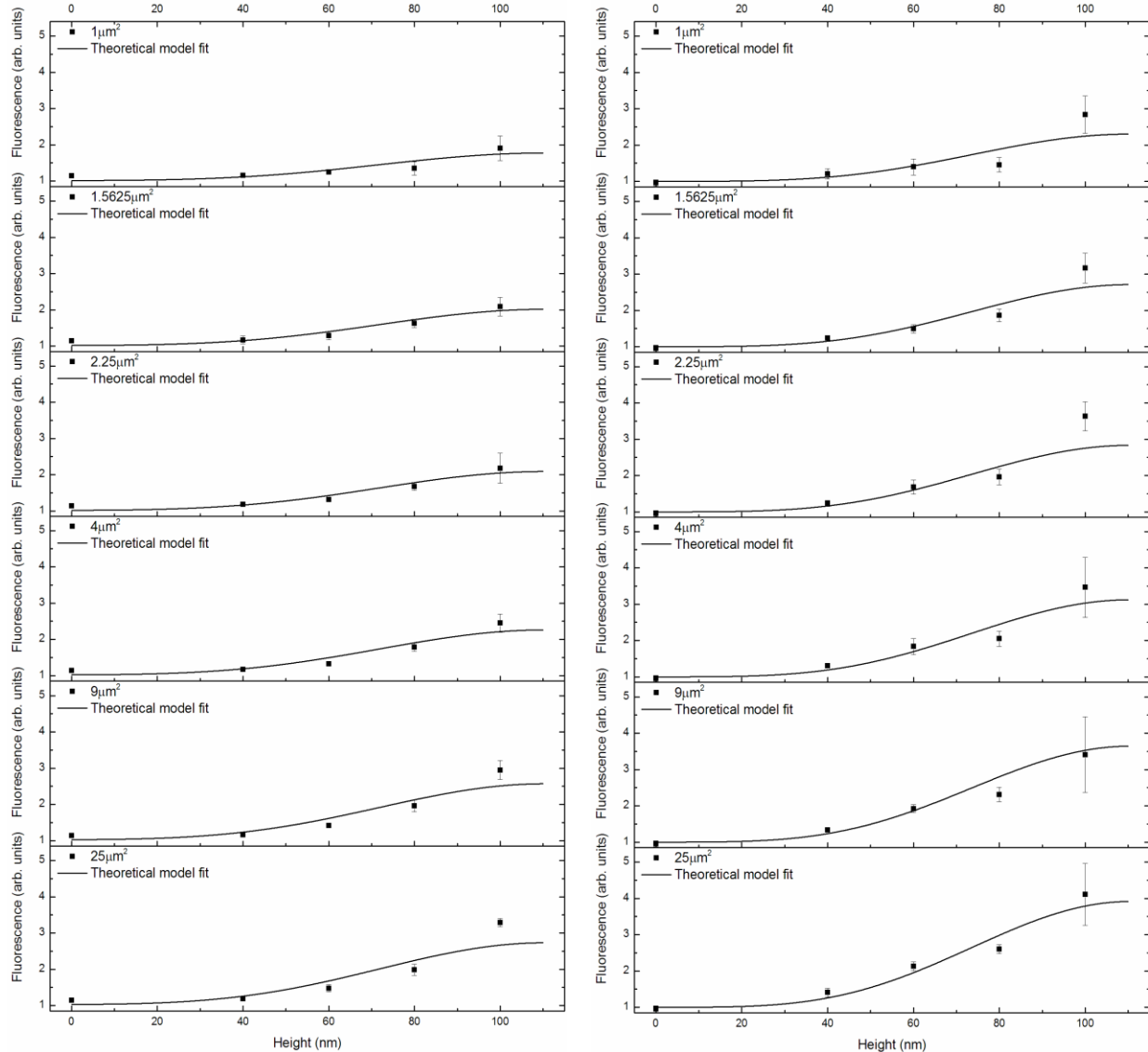


Figure SI 4. Fitting of the theoretical model curve on the experimental data (SiO_2/Si on the left, SiO_2/Pt on the right) for FLIC-enabled structures with the optimum height (100 nm).

The regression analysis correlating the fluorescence signal on structured surfaces with various parameters of these surfaces is presented in Figure SI 4. An inspection of the comparison between the amplification of the fluorescence signal for various footprints demonstrates that

larger one are capable to deliver an amplification of the fluorescence/unit area up to 4x, and 3x, for Pt-, and Si-based substrates, respectively, for FLIC structures with a footprint of $25 \mu\text{m}^2$, but only 2.5x, and 1.5x, for the same Pt-, and Si-based surfaces, but with FLIC structures having footprints of $1 \mu\text{m}^2$. This reduced amplification is remarkable, in particular as the top area of the FLIC structures per unit area, e.g., $100 \times 100 \mu\text{m}$, is identical for all footprints considered.

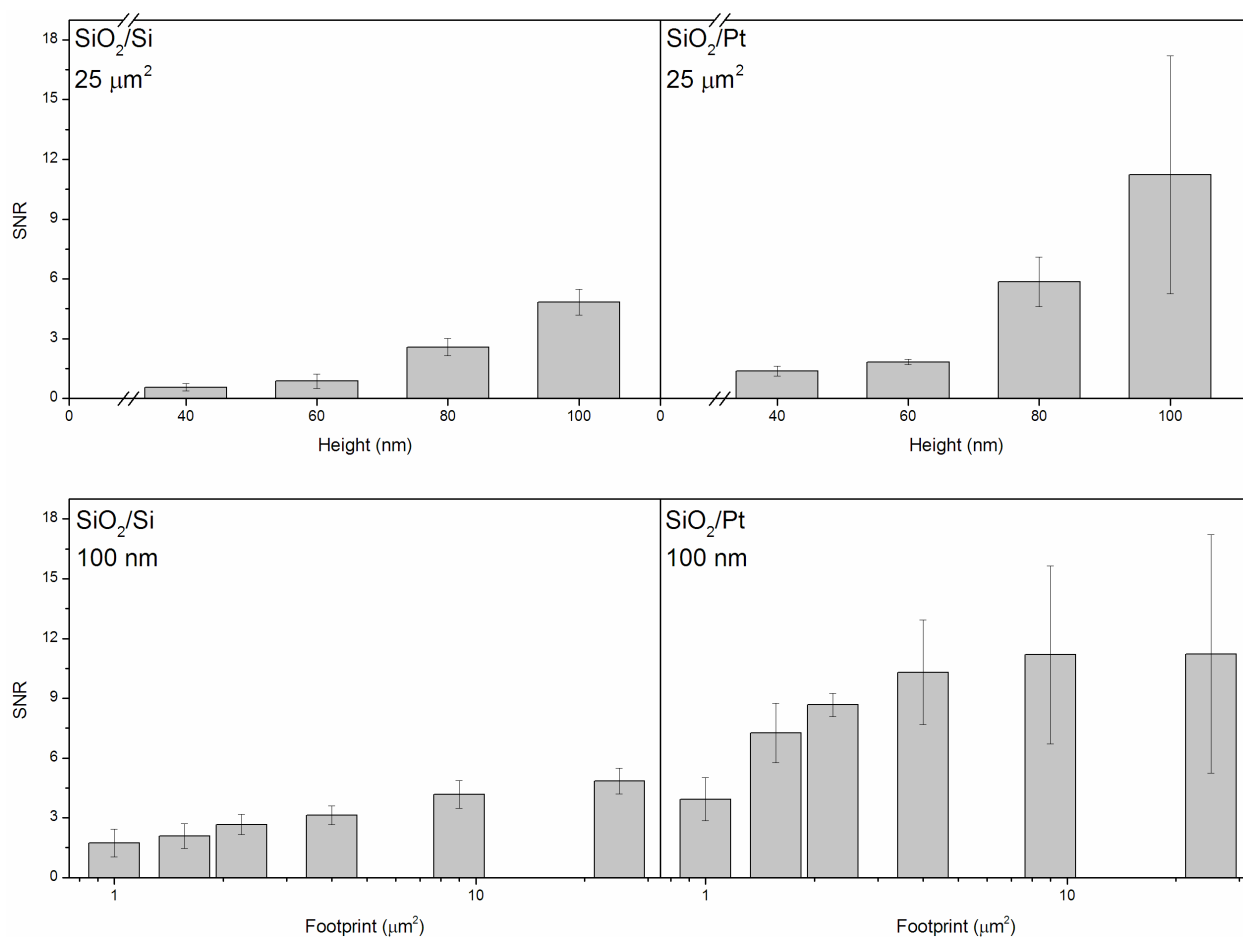


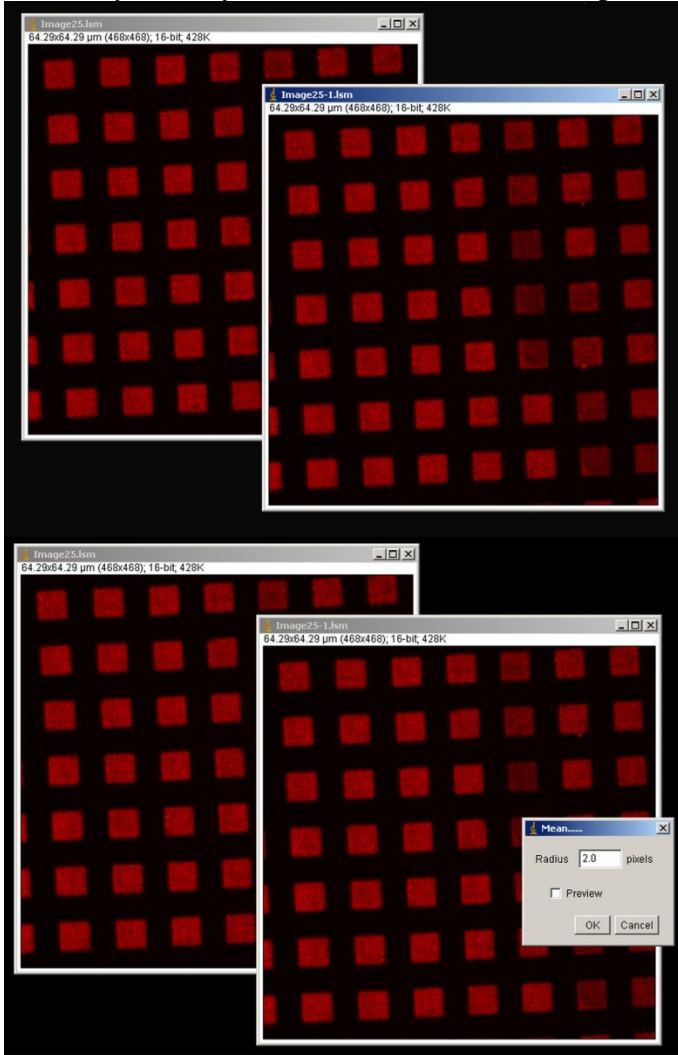
Figure SI 5. Signal/Noise Ratio, SNR, defined as the ratio between the fluorescence on the FLIC-enabled structures and the fluorescence outside the structures, as a function of the height of the structures (top, the largest footprint); and as a function of the footprint (bottom, the optimum height). SiO₂/Si on the left, SiO₂/Pt on the right.

5. Microarray image analysis and quantification

5.1. Segmentation and integration algorithm

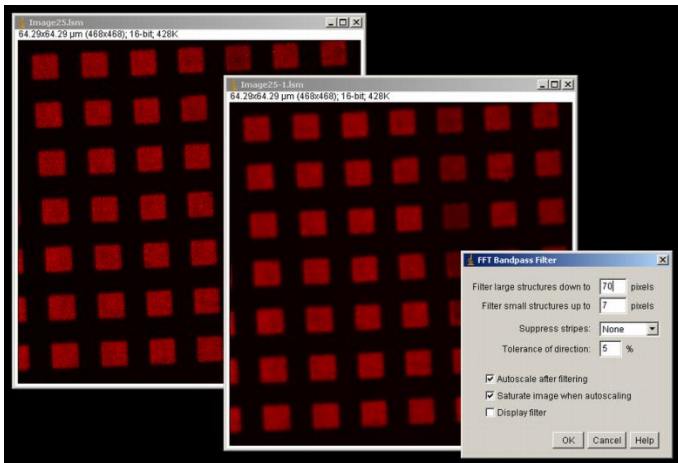
The procedure that was used to extract the quality data was described in the experimental section but deserves a more in depth description. The procedure applied for the spots printed on the flat substrates was straightforward, based on the Otsu thresholding algorithm (as implemented in ImageJ). This thresholding procedure is commonly used in microarray data extraction (Rueda and Rezaeian 2011). For the structured substrates however, the same type of thresholding is

initially applied to ensure non-biased identification the area where the sub-spots are. Further, a selection comprising a 3 x 3 array of 6 x 6 pixels is superimposed on a set of 9 sub-spots. Because this method relies on human intervention, additional qualifications are warranted. Firstly, the determination of the area where the sub-spots are located is automated. Secondly, within the area identified via thresholding, non-square sub-spots exist on the boundary of this region. The fact that these sub-spots are excluded is rooted in the underlying design concept of the substrates in that they provide a built-in structuring element. The substrate architecture proposed here addresses this issue by “forcing” spots (sub-spots here) to take a standard (known) shape and (known) size, based on the principle that it is computationally less complex to automatically identify features whose size and shape is known *a priori*.

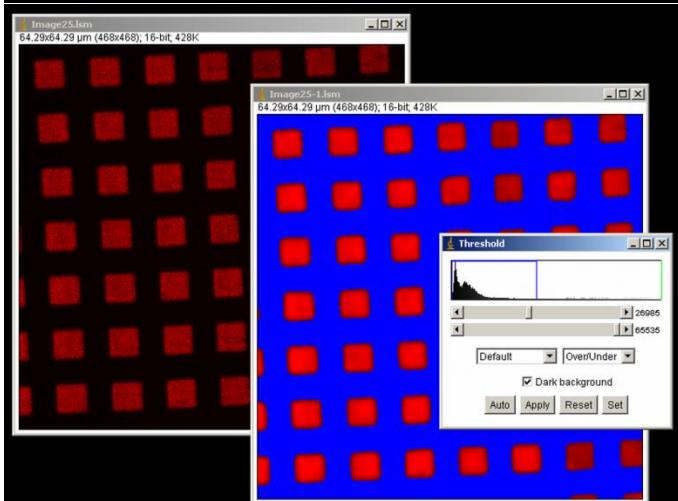


Original image in duplicate

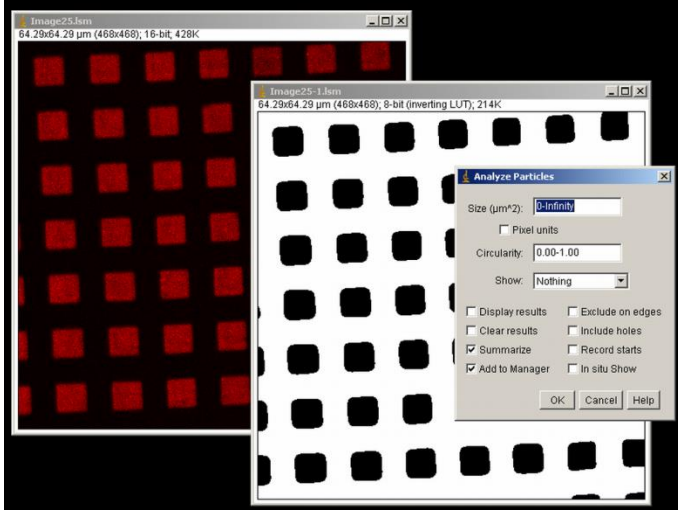
Application of a median filter



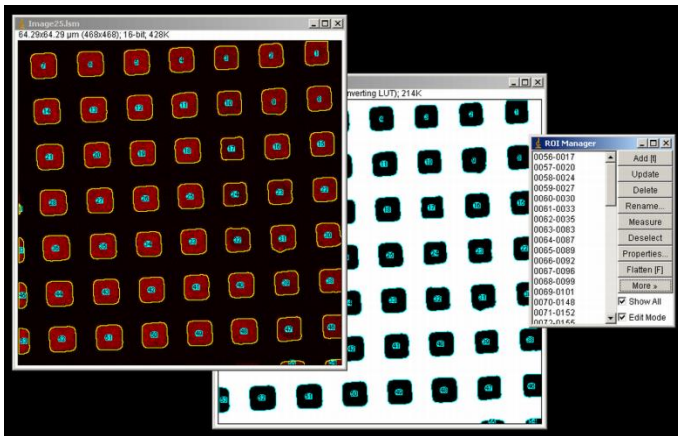
Application of a bandpass filter



Thresholded image



Binary image



Edge detection in the binary image and transfer of edge map to original image

Figure SI 6. The process of segmentation and quantification of microarray spots.

Within this framework, it is only natural that sub-spots with shapes different from the expected one (square) are excluded (albeit manually at this point). Thirdly, only a set of sub-spots is chosen from all the sub-spots that, through their shape and size, qualify for further analysis. But the sub-spots are selected using a fixed grid array containing 3 x 3 cells. The choice of number of array elements is not important as long as it delivers a statistically sufficient number of pixels (270 pixels in this case while the number of pixels per spot deemed statistically sufficient in the microarray literature ranges between a minimum of 25 (Dufva 2005) or, generally, a pixel size of a tenth of the spot diameter (Schna 2003)). The important aspect however is that the sub-spots are linked inside the array selection. That is, even if the positioning of the selection is biased with regards to one or two sub-spots (and even this assessment is on a visual basis), the array contains 9 elements and it is therefore highly improbable to purposely choose the best ones, let alone all of them fitting in the same 3 x 3 array.

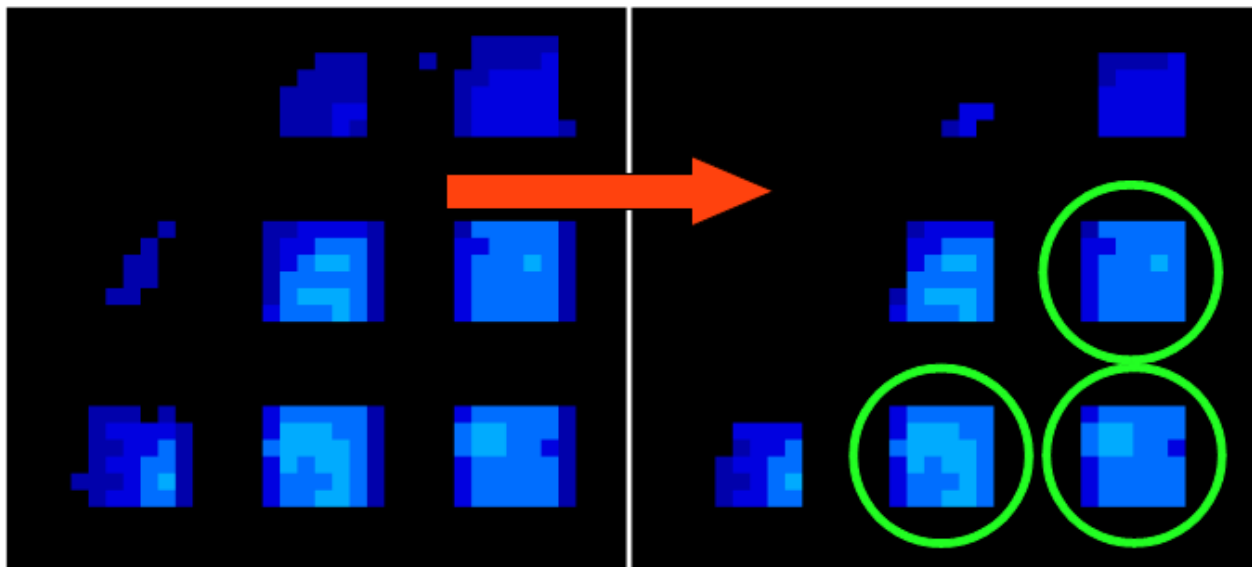


Figure SI 7: Only spots that, after thresholding, have the correct pre-defined shape (inside green circles) will be considered for data extraction

References to Supplementary Information

- Brandstatter, M., Fromherz, P., Offenhausser, A., 1988. Fluorescent Dye Monolayers on Oxidized Silicon. *Thin Solid Films* 160(1-2), 341-346.
- Dufva, M., 2005. Fabrication of high quality microarrays. *Biomol Eng* 22(5-6), 173-184.
- Habeeb, A.F.S., 1966. Determination of Free Amino Groups in Proteins by Trinitrobenzenesulfonic Acid. *Anal Biochem* 14(3), 328-&.
- Lambacher, A., Fromherz, P., 1996. Fluorescence interference-contrast microscopy on oxidized silicon using a monomolecular dye layer. *Appl Phys a-Mater* 63(3), 207-216.
- Lambacher, A., Fromherz, P., 2002. Luminescence of dye molecules on oxidized silicon and fluorescence interference contrast microscopy of biomembranes. *Journal of the Optical Society of America B: Optical Physics* 19(6), 1435-1453.
- Levinson, H.J., 2005. Confronting the diffraction limit. *Principles of lithography*, pp. xii, 423 p., 2nd ed. SPIE Press, Bellingham, WA.
- Luzinov, I., Julthongpipit, D., Liebmann-Vinson, A., Cregger, T., Foster, M.D., Tsukruk, V.V., 2000. Epoxy-terminated self-assembled monolayers: Molecular glues for polymer layers. *Langmuir* 16(2), 504-516.
- Nakache, M., Schreiber, A.B., Gaub, H., McConnell, H.M., 1985. Heterogeneity of Membrane Phospholipid Mobility in Endothelial-Cells Depends on Cell Substrate. *Nature* 317(6032), 75-77.
- Oblak, M., Prezelj, A., Pecar, S., Solmajer, T., 2004. Thiol-reactive clenbuterol analogues conjugated to bovine serum albumin. *Z Naturforsch C* 59(11-12), 880-886.
- Parthasarathy, R., Groves, J.T., 2004. Optical techniques for imaging membrane topography. *Cell Biochem Biophys* 41(3), 391-414.
- Rueda, L., Rezaeian, I., 2011. A fully automatic gridding method for cDNA microarray images. *BMC Bioinformatics* 12.
- Schena, M., 2003. Microarray manufacturing. In: Schena, M. (Ed.), *Microarray Analysis*, pp. 163-164. Wiley-Liss, Hoboken, NJ.